33RD CONGRESS
OF THE INTERNATIONAL COUNCIL
OF THE AERONAUTICAL SCIENCES
STOCKHOLM, SWEDEN, 4-9 SEPTEMBER, 2022

ICAS 2022 SWEDEN

NUMERICAL INVESTIGATION ON THE AERO-PROPULSION EFFECT OF DISTRIBUTED PROPULSION FOR V/STOL APPLICATION

Sichen SONG[1], Shuanghou DENG[1], Qingxi LI[2], Hongyu QIAO[1] & Yujin LU[1]

[1]College of Aerospace Engineering, Nanjing University of Aeronautics and Astronautics, Nanjing, 210016, People's Republic of China
[2]AVIC General Aircraft Research Institute, Zhuhai, People's Republic of China

Abstract

The distributed propulsion system is widely considered a disruptive technology in the aviation industry due to its remarkable potential in improving flight performances. Meanwhile, compared with the propeller that used in most distributed electric propulsion VTOL aircraft, the electric ducted fan system is able to increase the right boundary of speed envelope and provide greater efficiency for high cruise speed. The present study presents the results of the aero-propulsion integration benefits and its inner method for various EDF integrated concepts through calculating a large array of 2D-axi concepts.

Keywords: distributed propulsion, aerodynamics, V/STOL, aero-propulsion interaction

1. Introduction

To meet the stringent sustainability goals established by NASA and the European Commission, numerous aircraft concepts featuring distributed propulsion (DP) have appeared in recent decades [1–6]. DP systems promise improvements in, for example, aircraft's performance, noise reduction and provide V/STOL capabilities [7, 8]. By virtue of the similar power to weight ratio with different size of electric motors and the propulsive device can be separated from the power producing device, such as turbo-electric distributed propulsion (TeDP) concepts, hence, enable a high degree of integration of the airframe and propulsion system in aircraft design [9, 10].

Compared to numerous propeller-used DEP V/STOL aircraft, Electric Ducted Fan (EDF) increase the right side of speed envelope and provide greater high -speed efficiency. However, it is a great challenge to integrate the EDF that could balance between V/STOL and high-speed cruise performance. The main work of the present study is to design and evaluate a transport UAV equipped with TeDP and EDF, with a cruise speed 0.5 Ma in 3000m altitude. Besides, the V/STOL capability is also considered. Specifically, The aero-propulsive characteristics of engine-wing concept in transonic condition have been investigated by Lockheed Martin and AFRL [11]. To maximize the cruise efficiency, the engine is arranged under the trailing edge of the wing according to the research of the Dragon aircraft coming from Airbus and ONERA [12]. Moreover, ONERA has proposed a configuration with EDFs placed above the trailing edge [13], likely as Lilium jet. In addition, ECO-150 is one of the few aircrafts choosing split-wing propulsor design [14] (see Figure 1). For now, there is no clear conclusions or suggestion on the optimum location of engine arrangement in DP aircrafts.

In order to provide aerodynamic data supporting the general design phase, this paper investigates various EDF integrated concepts first in cruise condition, then approach and STOL condition and finally VTOL condition. The main phenomena and inner principles of the aero-propulsive characteristics are further studied.

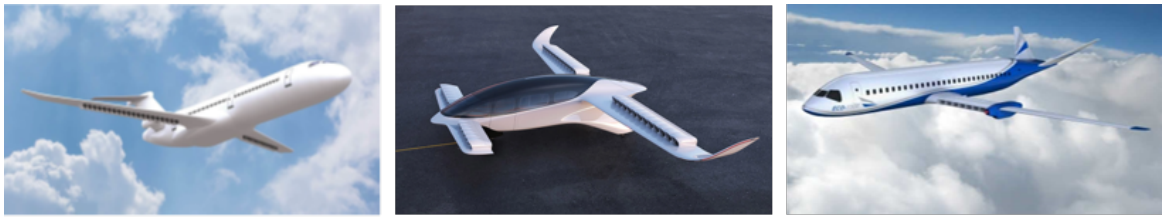

Figure 1 – Latest EDF-wing integration concepts.

2. Model and Computational Method

2.1 Test Model

To evaluate the aerodynamic performance of fan-wing integration effect, four flight phases, viz., cruise, approach, short takeoff and landing (STOL) and vertical takeoff and landing (VTOL), have been considered for the sake of exploring the aero-propulsion benefits of distributed propulsion configurations. The flight parameters for the aforementioned four flight phases are accordingly shown in Table 1 and Table 2. Among which, the parameters of STOL condition is referred to the shipborne rolling vertical landing (SRVL) method adopted by F-35B [15].

Table 1 – Flow parameters

	Velocity	Altitude, m	AoA, $^\circ$
Cruise	0.5 Ma	3000	3
Approach	0.15 Ma	300	8
STOL	29.25 m/s	50	12
VTOL	3 m/s	0	90

Table 2 – Fan parameters at pressure inlet boundary condition

	P_{total}, Pa	T_{total}, K	FPR
Cruise	89795	288.2	1.08
Approach	104299	291.4	1.05
STOL	110333	295.3	1.09
VTOL	111325	295.9	1.10

A typical computational model of the configuration is proposed to simplify the simulation, including a wing section and axisymmetric section of the EDF. The simulated configurations in this paper can be divided into upper and imbedded configuration, as shown in Figure 2. As for upper configurations, three detailed subitems based on a low drag natural laminar airfoil NACA64212 have been designed and named as Upfront, Upmiddle and Upback, according to the fan location along the wing chord. Referred to imbedded configuration, there are still three detailed configurations taken into consideration, such as Imbedded-LM, which has been proved according to reference [11], Imbedded-Test and Imbedded-Final.

Double slotted flaps are used for all upper and imbedded configurations in approach, STOL and VTOL conditions (see Figure 3), likely as the real aircraft. The Imbedded-LM and Imbedded-Test configurations were not downseclcted due to the poor performance, which will be described detailedly in next chapter. The main difference of the shape between the approach and STOL condition is the maximum deflecting angle of vanes and flaps, varying from 50° to 70°. For the VTOL condition, only upback and imbedded configurations are investigated as they are only two configurations with capability to totally deflect flow direction or thrust line.

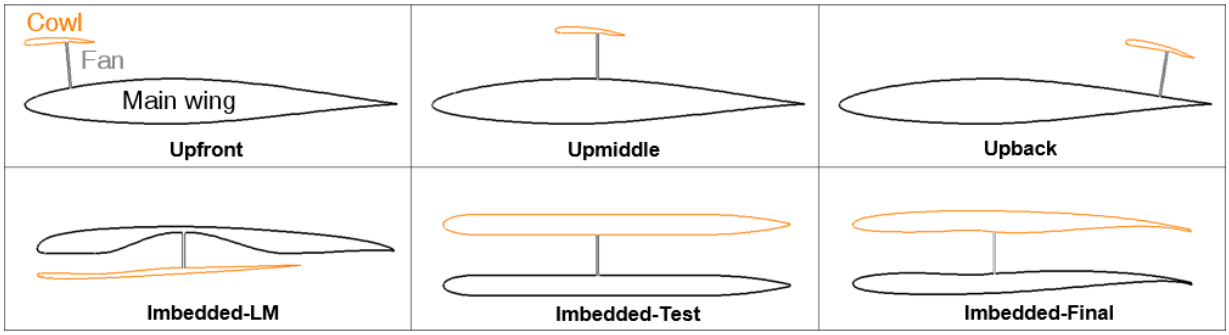

Figure 2 – The detailed upper and imbedded configurations.

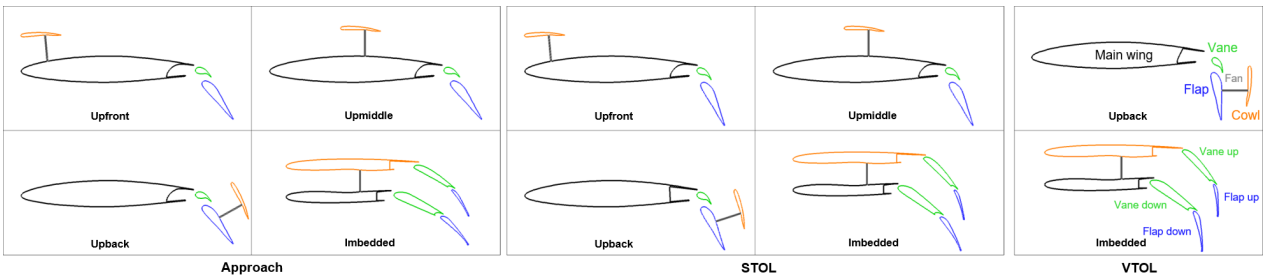

Figure 3 – Different positions of flaps on approach condition (left), STOL condition (middle) and VTOL condition (right).

2.2 Computational Method

Numerical simulations in the present study were carried out using commercial flow solver, ANSYS Fluent, which solves the 2D compressible Reynolds-Averaged Navier-Stokes (RANS) equations and enclosed by the two-equation $k-\omega$ shear stress transport (SST) turbulence model. A second-order upwind scheme for the viscid flux and a central difference scheme for the viscous flux were employed to discretize the governing equations, in which the gradients are reconstructed by the least square method.

Figure 4 shows the boundary conditions, where the size of computational domain is $22.5c \times 15c$ for the condition of cruise, approach and STOL, while the domain is $15c \times 15c$ for the condition of VTOL. A mass flow boundary condition is used to simulate the fan intake and a total temperature/total pressure boundary condition is used to model the exhaust flow, where the rotating inside the EDF is omitted [16]. The value of the pressure inlet boundary condition is determined by the ideal cycle gas circulation equations [17]. For mass flow outlet boundary, to meet the physical law, its value should be equal to the mass flow on the pressure inlet face [18] . Noted that in the condition of cruise, approach and STOL, the pressure farfield boundary condition is adopted, whereas, velocity inlet and pressure outlet boundary conditions are used for VTOL condition (see Figure 4).

In addition, the thrust-to drag bookkeeping is an vital consideration for this study in order to obtain the total axial force combined with fan thrust and aerodynamic thrust generated by wall. The thrust of the fan is computed as [19]:

$$T = \dot{m} \cdot \Delta v + (P_{\text{exit}} - P_{\text{inlet}}) \cdot A_{\text{fan}} \tag{1}$$

where $\dot{m}$ is the gas momentum flowing through fan; Δv is the speed difference crossing the fan disk; A_{fan} is area of the fan, which is set to $0.0576m^2$. P_{exit} and P_{inlet} are the static pressure on the fan disk exit and inlet surface respectively.

To validate the accuracy of the thrust-to-drag bookkeeping method, an off-the-shelf EDF with 250 mm diameter [20] is chosen as a validation case. The velocity field around the fan is displayed in Figure 5. Results have shown that the fan disk generates thrust 345.0N while aerodynamic force 251.6N is produced by cowl and core. The total thrust 596.61N results in a deviation less than 3.5% when compared with the experimental data measured by means of force balance.

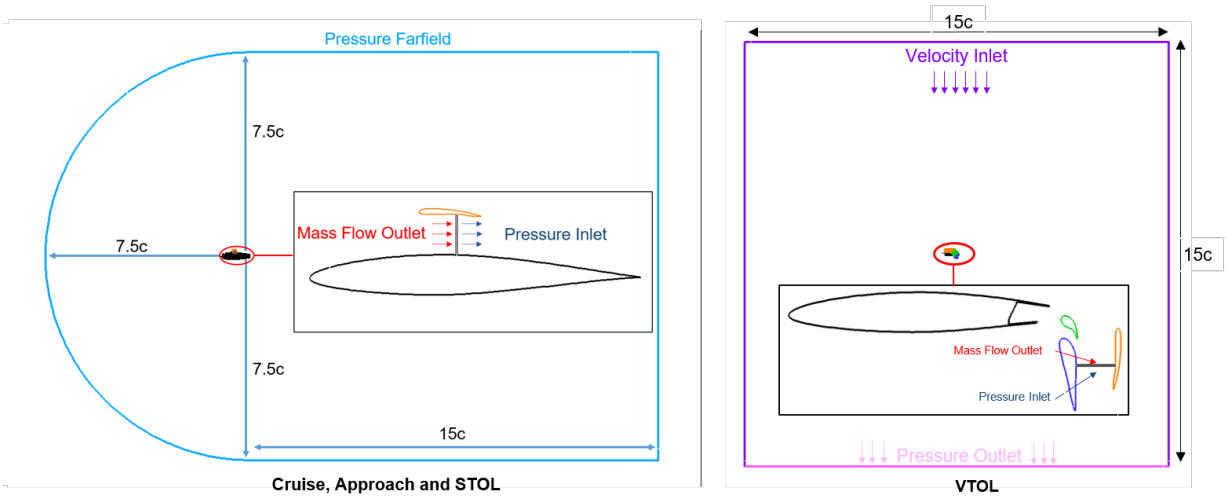

Figure 4 – Boundary conditions in cruise, approach, STOL conditions (left) and VTOL condition (right).

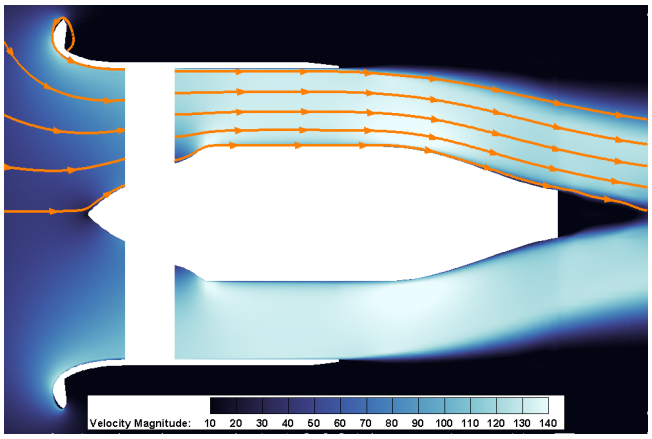

Figure 5 – The speed contour of validation case.

3. Results and Discussion

3.1 Cruise condition

3.1.1 Upper configuration

For the cruise condition, the flow and fan parameter in Table 1 and Table 2 were employed respectively. Figure 6 shows the aerodynamic force generation of the tested three upper configurations in Figure 2 with the comparison of the benchmark, the basic NACA64212 airfoil, where the dark color is the aerodynamic force generated by the entire system including the airfoil and up-mounted engine cowl, the light color represents the aerodynamic forces generated by the solo airfoil. Clearly, mounting the engine can in practical improve the lift due to the presence of the cowl, likely as the double wing concept. However, the lift generated on the wing decreases for the upfront configuration while the upmiddle and upback configurations increases significantly. Mounting the engine near the leading edge changes the pressure distribution on the front part of the suction surface on the wing where the suction pressure is decreased simultaneously as can be seen from Figure 7 and also evidenced in the pressure distribution in Figure 8. Moving to the upmiddle and upback configurations, the presence of the engine on upper surface accelerate the flow velocity and thus an extra low pressure region is created on the upper surface, particular for the upback configuration, see Figure 7 and 8. Moreover, mounting the engine on upper surface is able to influence the pressure on low surface of the wing slightly. Note that the main wing of upmiddle and upback configuration decrease the drag production and even to create thrust during cruise condition might because the main wing acts like the lip of turbofan cowl.

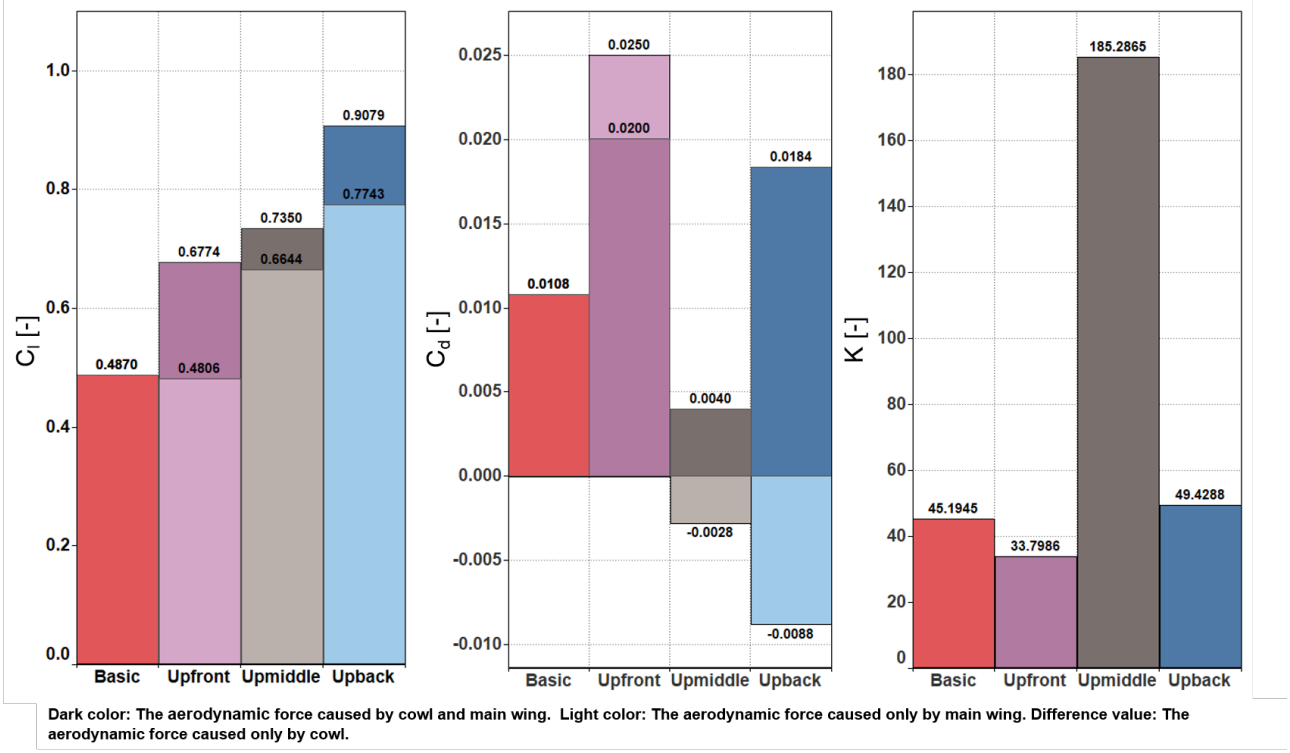

Figure 6 – Aerodynamic force of basic and upper configurations.

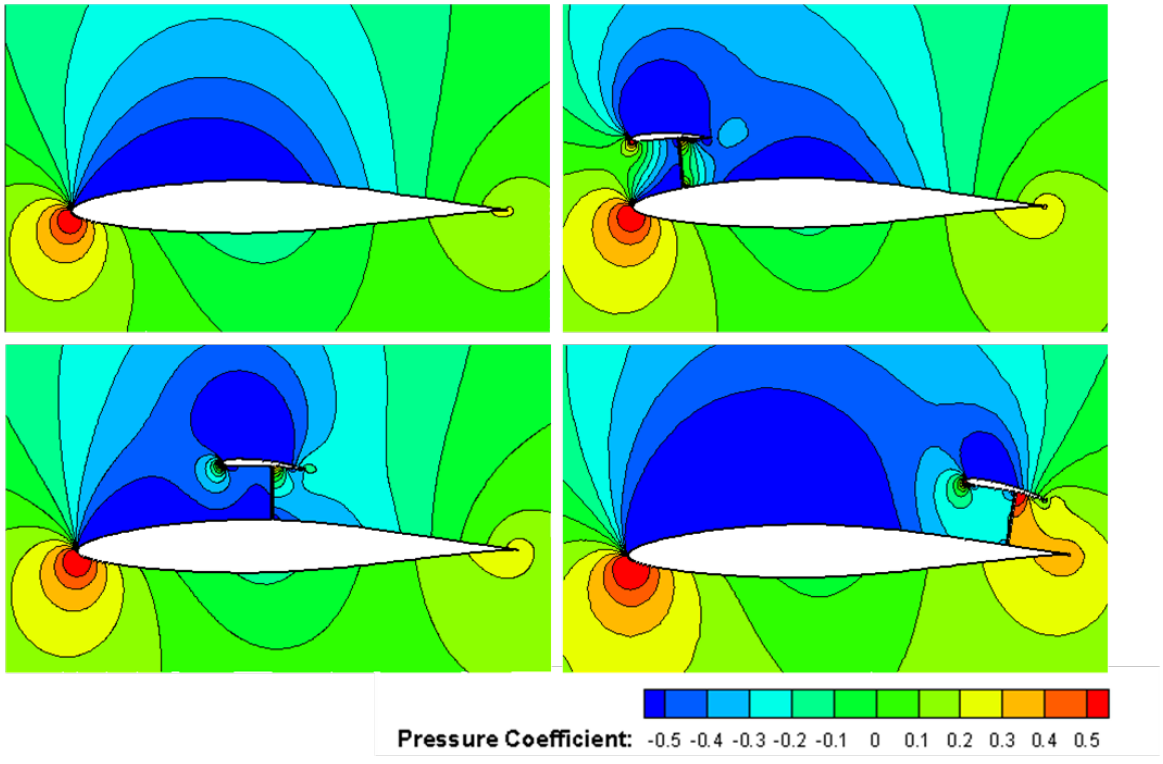

Figure 7 – Pressure coefficient contour of upper configurations.

3.1.2 Imbedded configuration

In the imbedded design, the leading edge and wing front half is converted into an inlet, while the wing stagnation region becomes a part of the propulsion area. The first imbedded configuration i.e., Imbedded-LM is proved in similar study [11]. However, the data in Figure 9 show that compared to upper configurations, Imbedded-LM configuration has a huge adverse in drag. Moreover, the down-wing creates tremendous downforce, resulting in a similar total aerodynamic lift force compared with

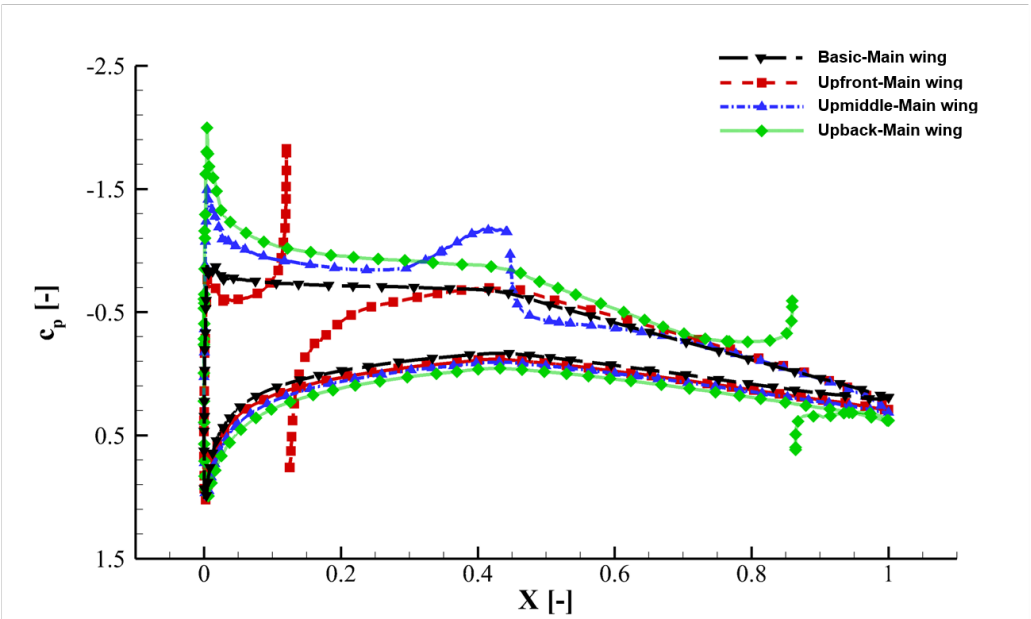

Figure 8 – Pressure distribution of upper configurations.

upback configuration, despite the lift created by up-wing is much greater than them, also the lift to drag ratio is far below.

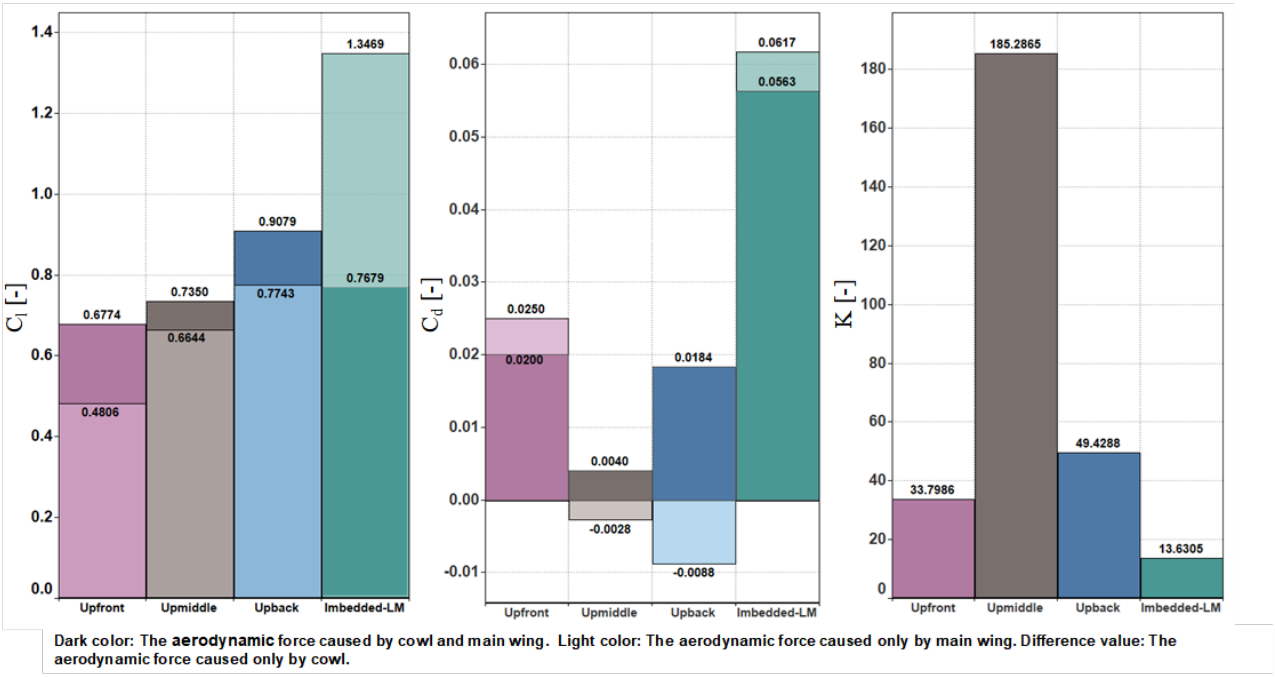

Figure 9 – Aerodynamic force of upper and Imbedded-LM configurations.

To explore the worst performance of Imbedded-LM configuration, the Imbedded-test configuration with the same symmetrical up-wing and down-wing was designed and simulated. Surprisingly, the result shown in Figure 10 indicates that Imbedded-test configuration has much lower drag and improves the ratio of lift to drag. According to the pressure distribution shown in Figure 11, the down-wing of Imbedded-test configuration generates majority of lift, that is the same for the up-wing of Imbedded-LM configuration, just as wing of aircraft. Meanwhile, the up-wing of Imbedded-test configuration generated a lot of downforce and thrust, as the down-wing of Imbedded-LM configuration. Hence, they are treated as cowl.

Moving to the pressure contour, Figure 12 obviously shows that the flow channel of fan in Imbedded-

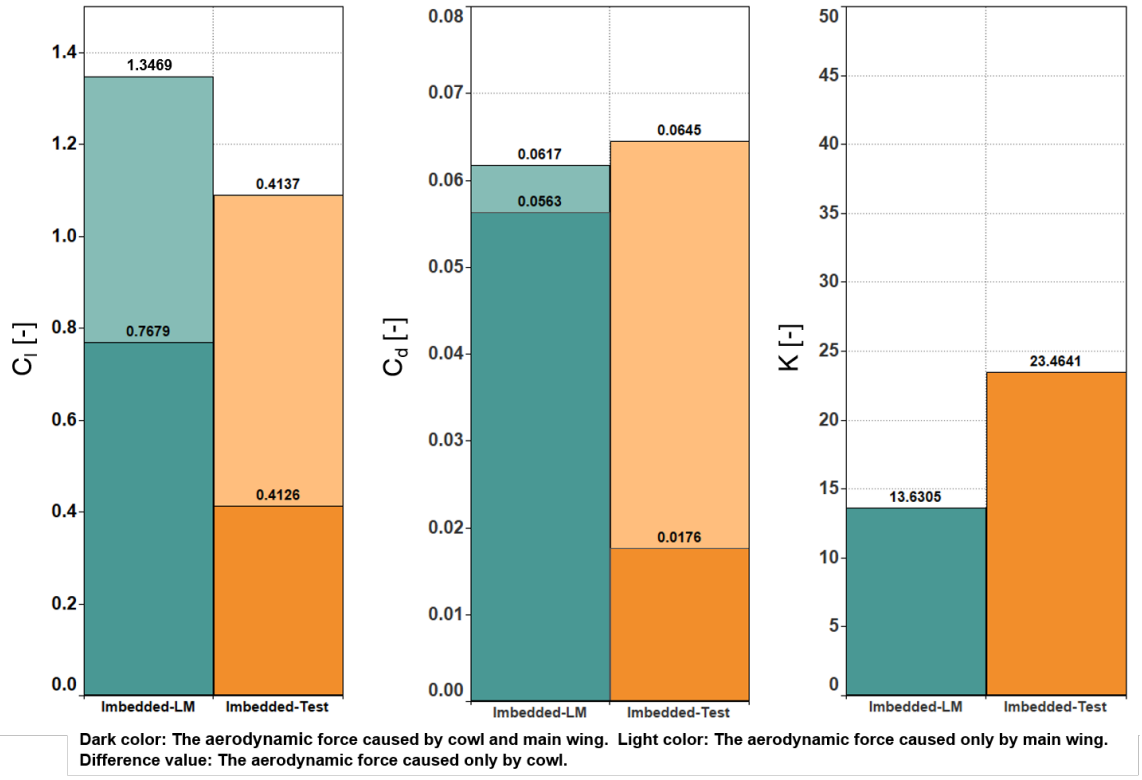

Figure 10 – Aerodynamic force comparison of Imbedded-LM and Imbedded-Test configurations.

test configuration generates a region with lower pressure compared with farfield. Alternatively, it is contrast to the Imbedded-LM configuration because the latter has a convergent nozzle which is able to reduce the mass flow rate and thus decrease the exhaust flow speed. One advantage of this effect is that a higher fan thrust can be achieved due to the higher pressure thrust. Considering the low speed performance might be improved by using externally blown flap (EBF), a high mass flow rate with high speed exhaust flow is required. Therefore, Imbedded-LM configuration in the present study is regarded as an optimum for cruise condition. Furthermore, the down-wing should be treated as main wing in design, likely as the Imbedded-test configuration.

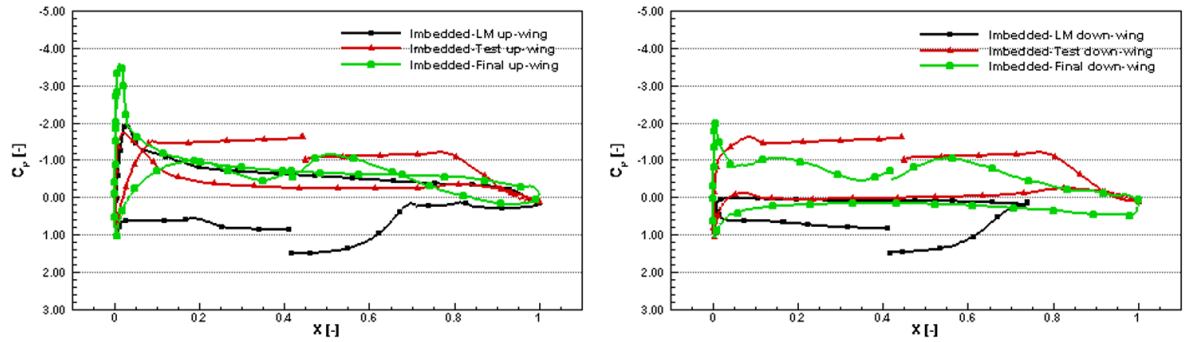

Figure 11 – Pressure distribution of Imbedded configurations.

Eventually, the Imbedded-Final configuration is designed with supercritical airfoil using both in the up-wing (NACA SC(2)-0707) and down-wing (NACA SC(2)-0710). The high pressure region on the aft lower surface could relieve the lift loss caused by the high speed jet, meanwhile a larger leading edge radius could provide an appreciable lip thrust. A slightly modification is applied in the flow channel to improve the intake and exhaust margin.

Both the up-wing and down-wing generate lift according to the calculation in Figure 13. As expected, down-wing generates majority lift force while up-wing generates lip thrust. Additionally, high pressure

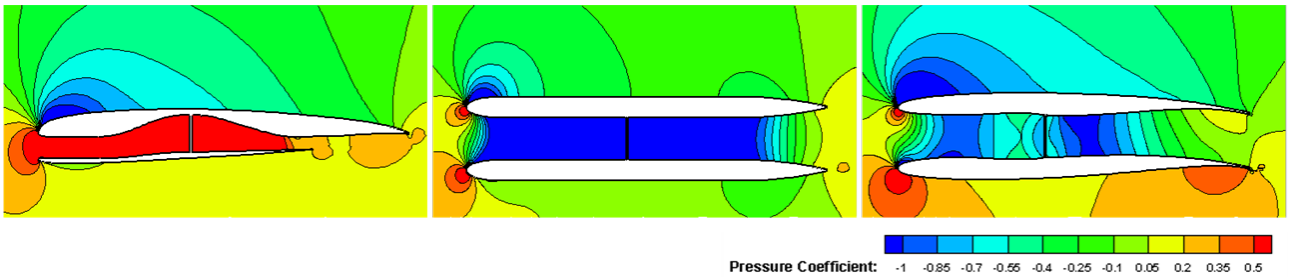

Figure 12 – Pressure coefficient contour of Imbedded configurations.

region on the aft lower surface is achieved in cowl. Consequently, one in Imbedded configuration that can compete with others in lift to drag ratio is designed. The pros of Imbedded-Final configuration is that small part of supersonic region can be seen in the leading edge region of the cowl and thus the drag increases a lot.

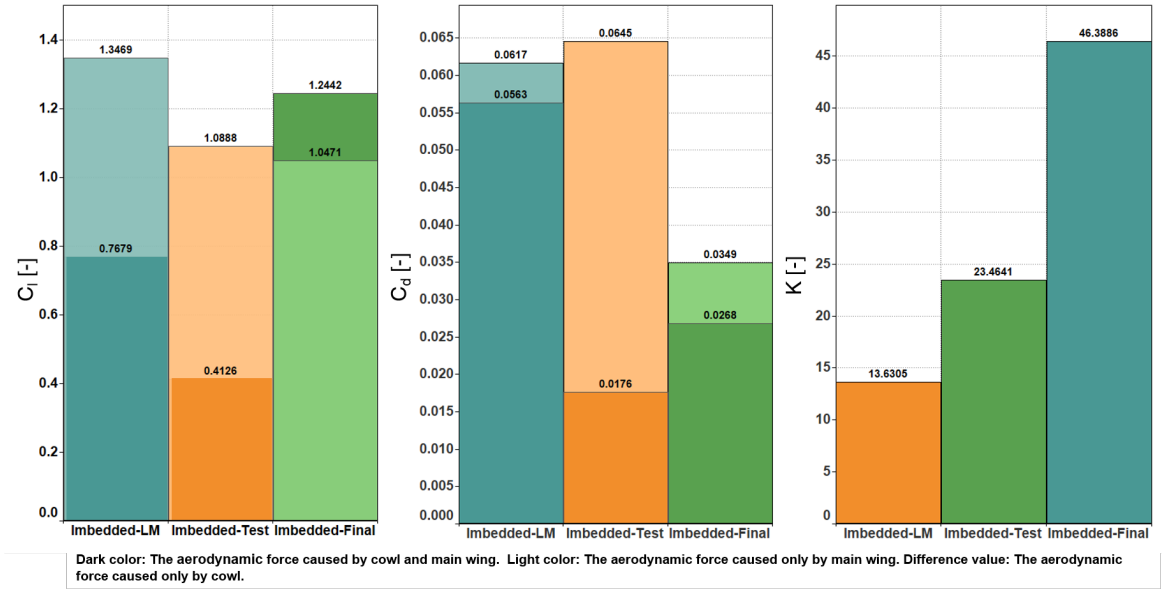

Figure 13 – Aerodynamic force of all Imbedded configurations.

3.2 Approach condition

All the upper and Imbedded-Final configurations have been chosen to proceed to the following condition for calculation. Models are shown in Figure 3, the farfield and fan boundary parameters used in this condition are shown in Table 1 and Table 2, respectively. Such condition represents the performance of final approach for aircraft. To fit the actual situation closely, all configurations have been designed with double slotted flap.

As shown in Figure 16(a), without the assistance of the slat, the flow separated in the leading edge undoubtedly as for the basic configuration , which is also relative to the characteristic of natural laminar airfoil. Moving to the upfront and upmiddle configurations, suction effect of fan takes over the slat, which results in the separated flow reattached to main wing before the fan disk surface. Moreover, high speed jet flow created by fan disk generates low pressure region when compared to the farfield. It is therefore, lift of main wing is improved. However, things go different in the upback configuration due to the mounted place of the fan. According to the Figure 16(d), the freestream flowing over the main wing acts like the basic configurations because the suction effect is not strong enough in such distance. Moving to the aerodynamic force shown in Figure 14, main wing of upfront configuration generates thrust and upback configuration increase substantially in main wing drag due to the suction effect affects the lower surface.

Despite the diminishing in lift and increasing in drag for main wing, one of the advantage is the high

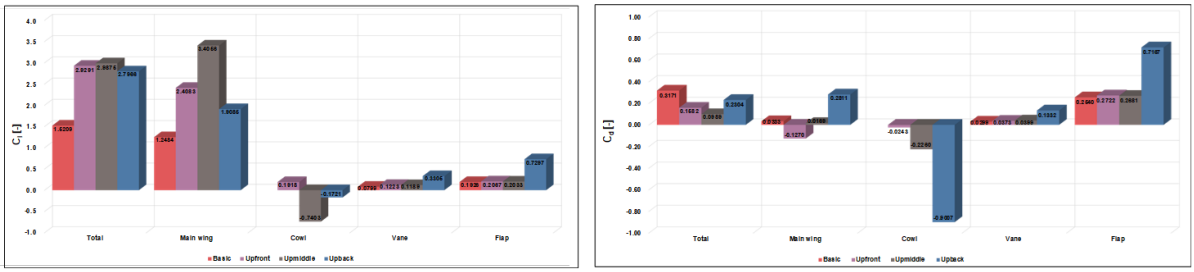

Figure 14 – Aerodynamic force of Upper configurations in approaching conditions.

lift generated in vane and flap, due to the suction effect works in this area for upback configurations. Nevertheless, the cost of high lift is high drag (see Figure 14). Another considerable effect is the thrust line for upback configurations that is totally different from others. Therefore, when the thrust component is added as shown in Figure 17, upback configuration possesses the highest lift and lowest thrust, which might be the most suitable for approaching condition requiring high drag and high lift.

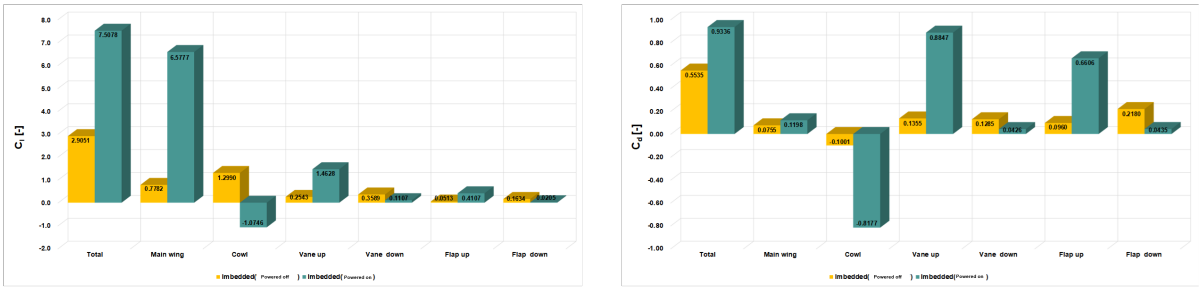

Figure 15 – Aerodynamic force of Upper configurations in approaching conditions.

Additionally, for the imbedded configuration shown in Figure 16 (e: power off) and (f: power on) , the EBF effect can be observed in the upside of vane and flap when power on. Meanwhile, the main wing generates a majority of lift due to the reason likely the same as the upfront and upmiddle configurations. Compared with the power off configuration, the lift is three times increase while the drag also augments nearly two times (see Figure 15). Similarly, adding the thrust component into the aerodynamic force, the result of imbedded configurations shows a far exceed lift than others and similar thrust level compared with upfront and upmiddle configurations at the same time.

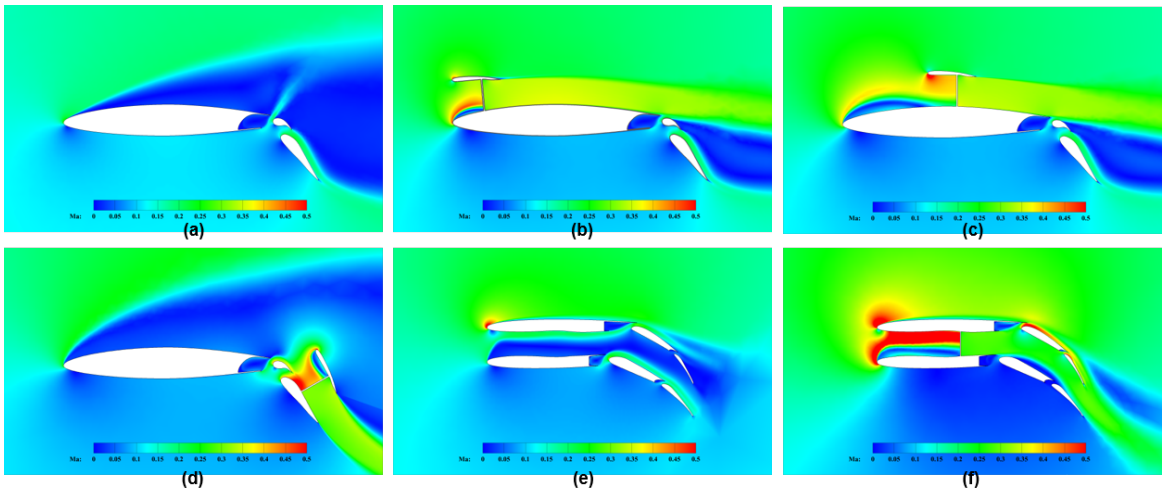

Figure 16 – Mach contour of configurations in approaching conditions.

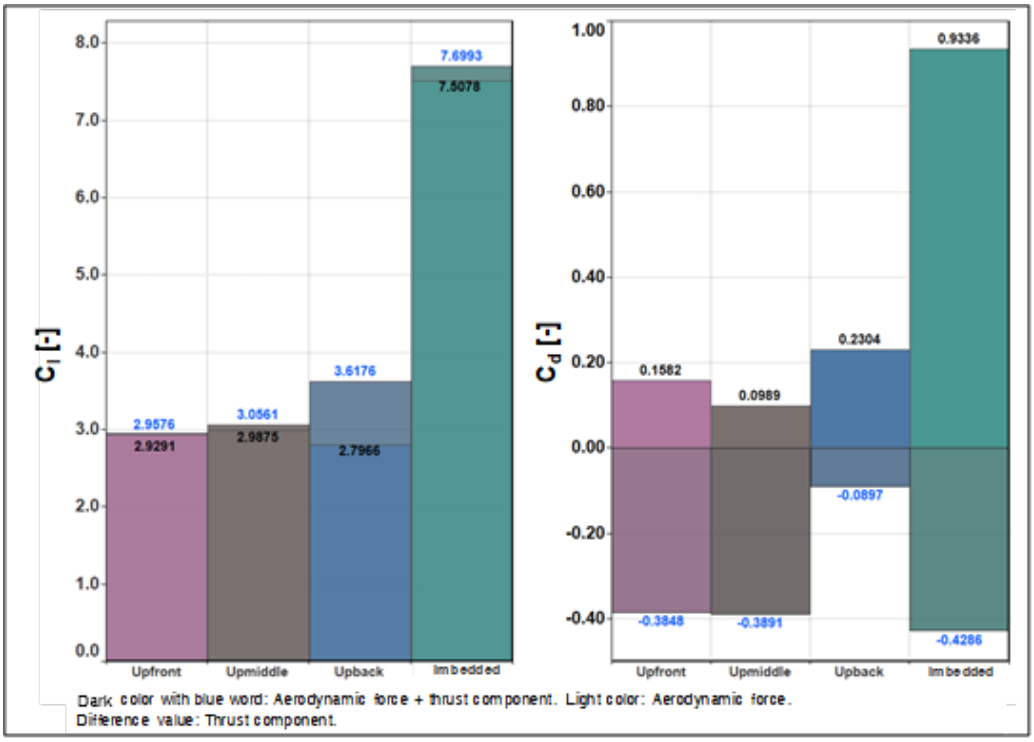

Figure 17 – Total lift and drag/thrust of Upper configurations in approaching conditions.

3.3 STOL condition

The main differences between STOL condition and approach condition is concluded as: (1) the higher fan pressure ratio or thrust in the same meaning; (2) the maximum deflection angle of double slotted flap raises 20 degrees.

When referred to the upper configurations, the flow structure and the aerodynamic force act as an enhanced version of approaching configuration (see Figure 18). The major difference is in drag, which generates negative drag or lip thrust in the same meaning because of the increasing FPR and thus the change of stagnation point in each surface.

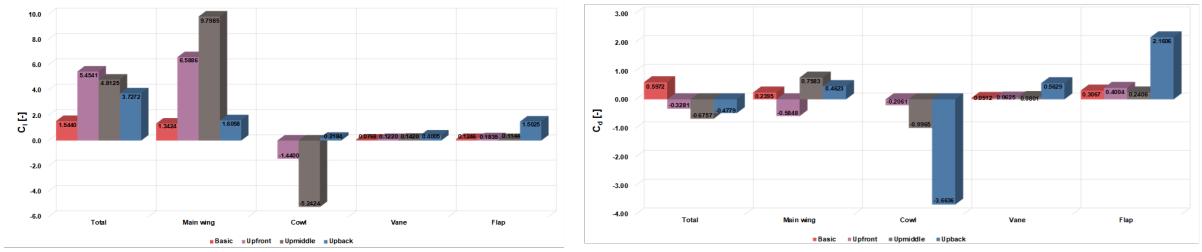

Figure 18 – Aerodynamic force of Upper configurations in STOL conditions.

Moving to the imbedded configuration, the EBF effect becomes stronger (see Figure 19). Note that the movement direction of the flow under the main wing is opposite to the freestream which is shown in the Figure 20 by the streamline. Fortunately, the vane and flap in downside prevent the fan disk sucking its exhaust flow to a large degree. Besides, a huge vortex is generated on the upper surface of the main wing, caused by both the stronger suction effect of fan and flow separation in the leading edge. High speed backflow in the vortex near the wall of main wing generates a low pressure region. Therefore, the main wing generates enormous lift compared with the power off configuration and even the power on model in approaching condition unsurprisingly.

After adding the thrust component, the lift generated by Imbedded configuration is much larger than others, while upmiddle configuration generates the highest thrust for the entire aero-propulsion system (see Figure 21). Note that the separation flow in the inlet for the imbedded flow indicates the performance degradation or even the risk of stall for the fan disk. And thus an effective way to solve

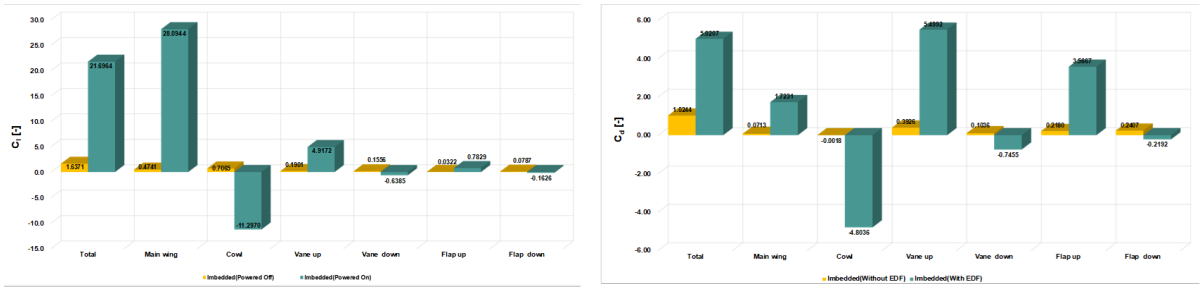

Figure 19 – Aerodynamic force of Upper configurations in STOL conditions.

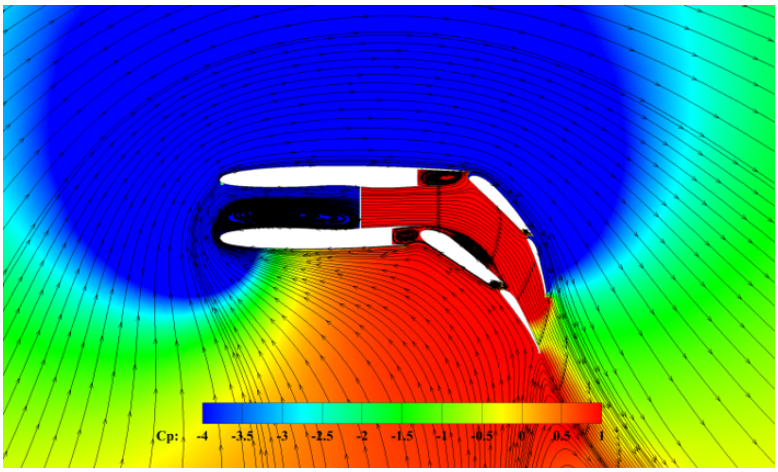

Figure 20 – Streamline in Imbedded configuration with power on.

this problem is to use centrifugal ducted fan or add slat for the main wing.

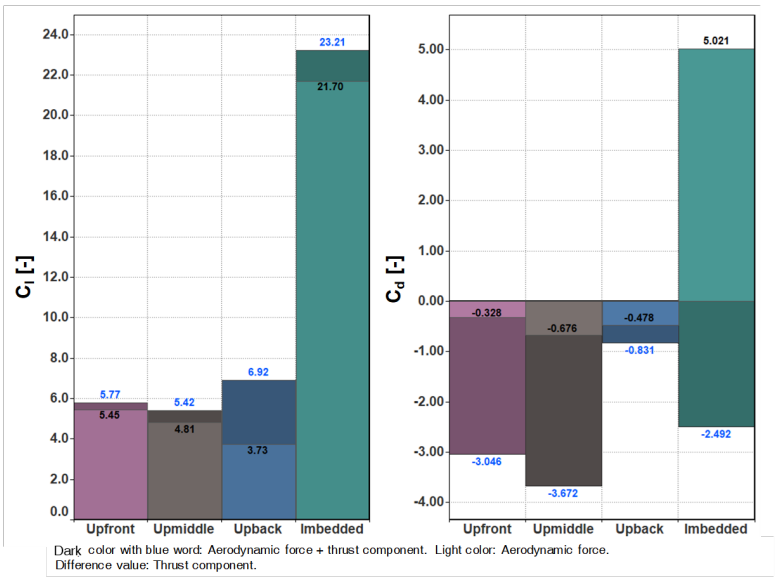

Figure 21 – Total lift and drag/thrust of Upper configurations in STOL conditions.

3.4 VTOL condition

As for the upper configurations, upfront and upmiddle configurations show a poor capability in lift increase by using upper surface blowing partly as the wrong extended place of vane and flap. Whereas, other two configurations perform the potential possibility to change thrust line or the exhaust flow direction. Thus, upback and imbedded configurations, shown in Figure 3, have been chosen in the present study.

Aerodynamic force in Figure 22 shows that the main wing generates downforce in upback configuration while other surfaces generate lift. According to the pressure contour in Figure 23, the stagnation point of main wing is on the upper surface, causing vortex right under the main wing with the assistance of the noticable suction effect caused by the fan disk. The leading edge of flap in upback configuration generates the majority of lift, working as the lip in turbofan engine cowl.

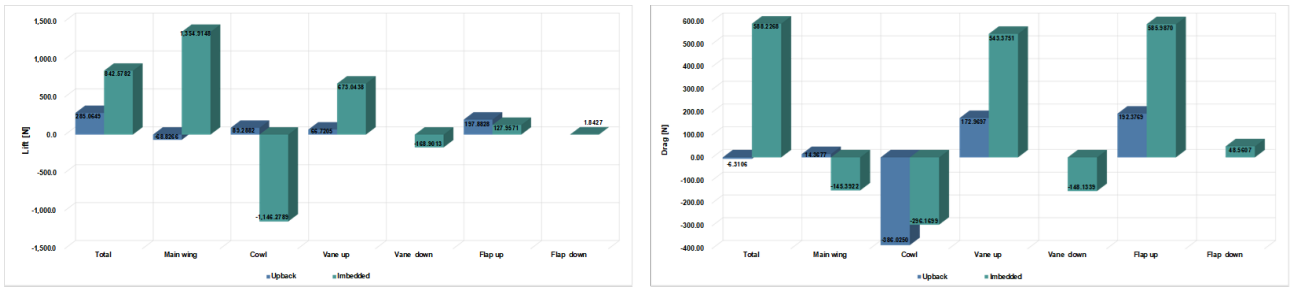

Figure 22 – Aerodynamic lift and drag of all configurations in VTOL conditions.

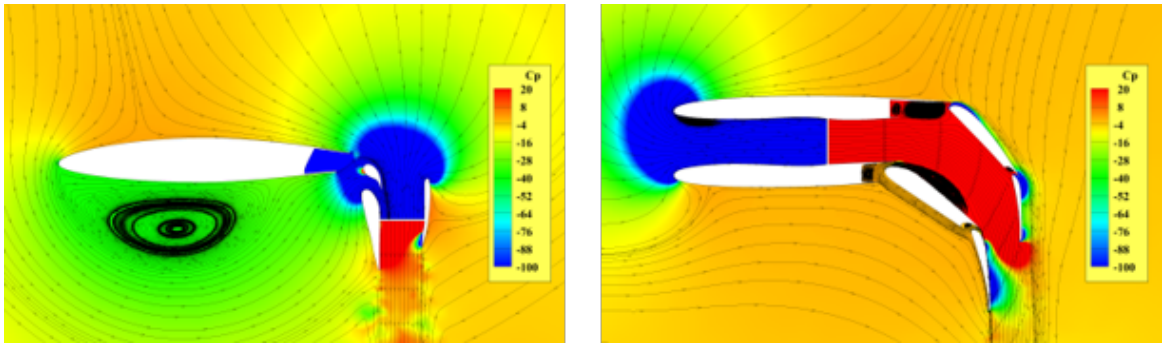

Figure 23 – Streamline and pressure comparison with configurations in VTOL conditions.

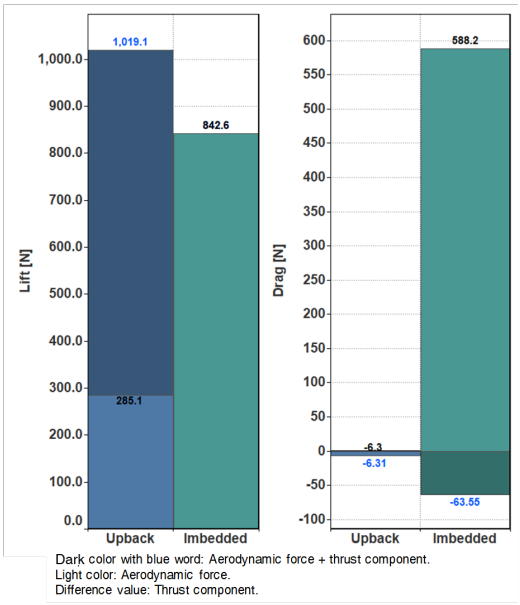

Figure 24 – Total lift and drag/thrust of all configurations in VTOL conditions.

As for imbedded configuration, the majority of lift is generated by the main wing and followed by the vane up. Alternatively, the cowl and vane down generate downforce. As seen in the pressure contour, strong suction creates low pressure region near the inlet. However, this phenomenon is adversely to the cowl. In addition, EBF effect does not only generate lift, but also deflect the flow direction to

reduce the total axial force for preventing the aircraft goes forward for VTOL condition. One failure design point is the downside flap and vane are not beneficial from EBF effect.
One key indicator of this working condition is the total lift, which is the aerodynamic lift plus the direct lift produced by the fan. In figure 24, it can be seen that the upback configuration improves the total lift by 21%. Imbedded configuration meanwhile generates nearly ten times axial force than the upback configuration due to the insufficient deflection angle of vanes and flaps. Obviously, the drawback of the upback configuration is the difficulty of structural design, thus might be overweighted compared with the imbedded configuration.

4. Conclusion

The present study performs numerical simulation on an integrated DP systems and evaluate various configurations in cruise condition and trade effect of fan location along the wing chord. Results show that the upback configuration generates the maximum lift in main wing while it is able to maximize thrust generation. The upmiddle configuration has the best lift to drag ratio for the aero-propulsion system due to the minimum cruise drag. The Imbedded configuration generates more thrust than upper configurations in cruise. The upper configurations and Imbedded-Final configuration were downselected for follow-on simulations.
The aerodynamic performance of all the tested configurations are similar in approach and STOL conditions. In which the Imbedded configuration is optimum in lift followed by the upback configurations. From the view of thrust-drag bookkeeping, all the tested configurations generate appreciable axial force except for the upback configuration scenario. Unfortunately, in approach and STOL conditions, lower axial force would be better for the aircraft, especially for approaching and landing stage.
For VTOL condition, upback and imbedded configurations were downselected for this simulations. All the configurations generate more lift compared with fan disk. However, there is no thrust loss in upback configuration and thus the total lift which calculated by thrust plus aerodynamic lift is 20% higher than imbedded configuration, where the lift is only generated by the aerodynamic force.

5. Acknowledgements

The present work is funded by Postgraduate Research and Practice Innovation Program of Jiangsu Province (SJCX22-0094). The third author acknowledges the support from Fundamental and Applied Fundamental Research of Zhuhai City(Grand no. ZH2201-7003-210011-P-WC) and AG-EX-JSXY-009.

6. Contact Author Email Address

Mail to: shuanghoudeng@nuaa.edu.cn

7. Copyright Statement

References

[1] Vries R D, Brown M and Vos R. Preliminary sizing method for hybrid-electric distributed-propulsion aircraft. *Journal of Aircraft*, Vol. 56, No.6, pp 2172-2188, 2019.

[2] Borer, N K, Patterson, M D, Viken, J K, Moore, M D, Bevirt, J, Stoll, A M and Gibson A R. Design and performance of the NASA SCEPTOR distributed electric propulsion flight demonstrator. *16th AIAA Aviation Technology, Integration, and Operations Conference*, Washington, D.C., AIAA 2016-3920, 2016.

[3] Rothaar, P M, Murphy, P C, Bacon, B J, Gregory, I M, Grauer, J A, Busan, R C and Croom, M A. NASA Langley distributed propulsion VTOL tilt-wing aircraft testing, modeling, simulation, control, and flight test development. *14th AIAA Aviation Technology, Integration, and Operations Conference*, Atlanta, GA, AIAA 2014-2999, 2014.

[4] Hermetz, J, Ridel, M and Döll, C. Distributed electric propulsion for small business aircraft: a concept-plane for key-technologies investigations. *30th Congress of the International Council of the Aeronautical Sciences*, Daejeon, Republic of Korea, ICAS Paper 2016-0461, 2016.

[5] Steiner, H J, Seitz, A, Wieczorek, K, Plötner, K, Iskiveren, A T and Hornung, M. Multi-disciplinary design and feasibility study of distributed propulsion systems. *28th Congress of the International Council of the Aeronautical Sciences*, Brisbane, Australia, ICAS Paper 2012-1.7.5, 2012.

[6] Voskuijl, M, van Bogaert J, and Rao A G. Analysis and design of hybrid electric regional turboprop aircraft. *CEAS Aeronautical Journal*, Vol. 9, No. 1, pp. 15–25, 2018.

[7] Brelje B J and Martins J R. Electric, hybrid, and turboelectric fixed-wing aircraft: A review of concepts, models, and design approaches. *Progress in Aerospace Sciences*, Vol. 104, pp 1-19, 2019.

[8] Gohardani A S, Doulgeris G and Singh R. Challenges of future aircraft propulsion: A review of distributed propulsion technology and its potential application for the all electric commercial aircraft. *Progress in Aerospace Sciences*, Vol. 47, No.5, pp 369-391, 2011.

[9] Moore M D. Misconceptions of electric aircraft and their emerging aviation markets. *52nd Aerospace Sciences Meeting*, Maryland, AIAA 2014-0535, 2014.

[10] Pelz P F, Leise P and Meck M. Sustainable aircraft design — A review on optimization methods for electric propulsion with derived optimal number of propulsors. *Progress in Aerospace Sciences*, Vol. 123, pp 100714, 2021.

[11] Wick A T, Hooker J R and Zeune C H. Zeune. Integrated aerodynamic benefits of distributed propulsion. *53rd AIAA Aerospace Sciences Meeting*, Kissimmee, Florida, AIAA 2015-1500, 2015.

[12] Schmollgruber P, Donjat D, Ridel M, Cafarelli I, Atinault O, François C and Paluch B. Multidisciplinary design and performance of the ONERA hybrid electric distributed propulsion concept (DRAGON) *AIAA Scitech 2020 Forum*, Orlando, Florida, AIAA 2020-0501, 2020.

[13] Sgueglia A, Schmollgruber P, Bartoli N, Atinault O, Benard E and Morlier J. Exploration and sizing of a large passenger aircraft with distributed ducted electric fans *2018 AIAA Aerospace Sciences Meeting*, Kissimmee, Florida, AIAA 2018-1745, 2018.

[14] Schiltgen B T and Freeman J. Aeropropulsive interaction and thermal system integration within the ECO-150: a turboelectric distributed propulsion airliner with conventional electric machines *16th AIAA Aviation Technology, Integration, and Operations Conference*, Washington, D.C., AIAA 2016-4064, 2016.

[15] F-35 helmet cam footage of shipborne rolling vertical landing (SRVL). `https://www.youtube.com/watch?v=e0ICnphzdJA`.

[16] Xiao T, Zhu Z, Deng S, Gui F, Li Z and Zhou Z. Effects of nozzle geometry and active blowing on lift enhancement for upper surface blowing configuration. *Aerospace Science and Technology*, Vol. 111, pp 106536, 2021.

[17] Gas turbine analysis - aerodynamics for students. `http://www.aerodynamics4students.com/propulsion/gas-turbine-analysis`.

[18] Zhi H, Zhu Z, Lu Y, Deng S and Xiao T. Aerodynamic performance enhancement of co-flow jet airfoil with simple high-lift device. *Aerospace Science and Technology*, Vol. 34, No 9, pp 143-155, 2021.

[19] Hirose N, Asai K, Ikawa K and Kawamura R. Euler flow analysis of turbine powered simulator and fanjet engine. *Journal of Propulsion and Power*, Vol. 7, No. 6, pp 1015-1022, 1991.

[20] Vsay fan VF-250 EDF. `https://www.vasyfan.com/EdfPlus/PlusVF250SA.html?lng=EN`.